ELSEVIER

Journal of Nuclear Materials 278 (2000) 195–201

journal of nuclear materials

www.elsevier.nl/locate/jnucmat

Oxidation of β-Nb and $Zr(Fe, V)_2$ precipitates in oxide films formed on advanced Zr-based alloys

Dominique Pêcheur *

CEA-Cadarache, DRN/DEC/SH2C, bât.224, 13108 Saint Paul Lez Durance cedex, France

Received 7 June 1999; accepted 1 October 1999

Abstract

The incorporation of precipitates β-Nb and $Zr(Fe, V)_2$ into the oxide films formed on advanced Zr-based alloys (Zr–1%Nb and Zr–0.5%Sn–0.6%Fe–0.3%V) is studied by transmission electron microscopy, on cross-sectional thin foils. The main results are: (1) the oxidation of both precipitates is delayed compared to the zirconium matrix, (2) the precipitates remain unoxidized in the inner part of the oxide layer, up to about 300 nm from the metal–oxide interface. In another terms, they undergo no modification (neither structural nor chemical) in the innermost part of the oxide film, (3) the chemical composition of precipitates evolves during their oxidation. These results are compared to previous results dealing with the incorporation of $Zr(Fe, Cr)_2$ precipitates into the oxide layer of Zircaloy-4 and discussed in relation to the oxidation process.

1. Introduction

In light water reactors, the waterside corrosion of cladding materials is one of the main limitations to the extension of fuel rod burnups. Among metallurgical parameters which influence the oxidation resistance, the second phase particles are known to play a critical role. To improve the understanding of their role in the corrosion process, few authors have investigated their oxidation behaviour using transmission electron microscopy [1–5] and, recently, Auger analysis [6,7]. Most of the investigations were conducted on $Zr(Fe, Cr)_2$ precipitates contained in Zircaloy-4 material.

The main results are that the oxidation of the $Zr(Fe, Cr)_2$ intermetallic precipitates is delayed compared to the zirconium matrix. They are incorporated unoxidized into the oxide film, and no iron nor chromium depletion is observed inside the precipitates. They are later oxidized to cubic (or tetragonal) ZrO_2 in the outer part of the oxide film. Their oxidation is then accompanied by a partial iron dissolution in the ZrO_2 matrix.

The present work also performed by TEM, is an extension of the previous study (focused on $Zr(Fe, Cr)_2$ precipitates) to other types of precipitates: β-Nb and $Zr(Fe, V)_2$ which are present in advanced Zr-based alloys.

2. Experimental procedure

Three materials, all supplied by Framatome, were studied in this work: standard Zircaloy-4 AFA2G and two advanced Zr-based alloys, alloy 4 (Zr–0.5%Sn–0.6%Fe–0.3%V) and alloy 5 (Zr–1%Nb). Their fabrication process and chemical composition are described in [8,9].

Oxidation tests were performed in the REGGAE out-of-pile loop, on as-received tubes, without performing any chemical surface preparation. This type of facility simulates the PWRs operating conditions except for the neutron flux, the rods corroded in the loop being electrically heated. The oxidation conditions were the followings: 190 bar, 636 K, 100 W/cm^2, Li = 5 to 10 ppm, B = 650 ppm, $O_2 < 1$ ppb.

The oxide films were analysed using a transmission electron microscope (Philipps EM 420 120 kV), fitted with an EDX sensor (for X-ray dispersive analysis). The

* Tel.: +33-4 42 25 45 60; fax: +33-4 42 25 29 10.
E-mail address: pecheur@drncad.cea.fr (D. Pêcheur).

0022-3115/00/$ - see front matter
PII: S0022-3115(99)00253-6

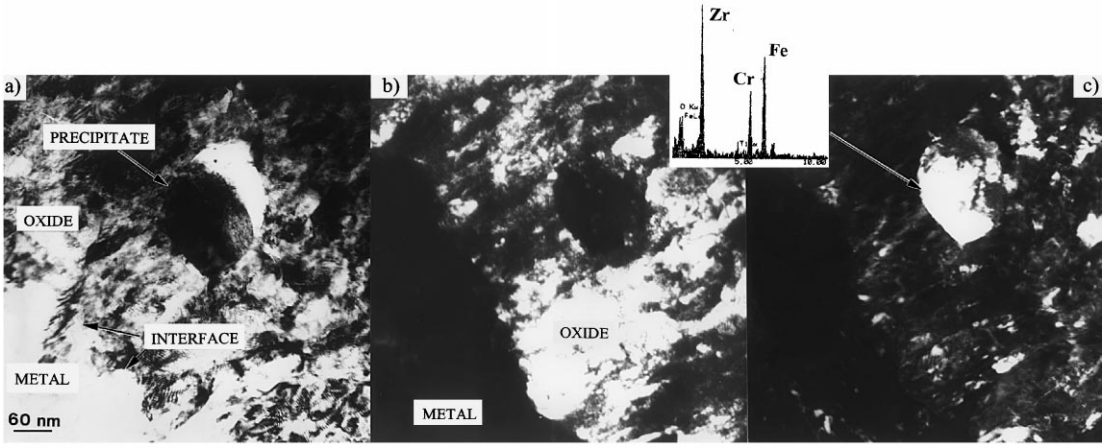

Fig. 1. Unoxidized $Zr(Fe, Cr)_2$ precipitate observed in the Zircaloy-4 oxide film, at about 250 nm from the metal–oxide interface: (a) bright field of the precipitate, (b) dark field of the oxide grains, (c) dark field of the precipitate.

thin foils were prepared in cross-section (e.g. observation plane perpendicular to the metal–oxide interface). Only post-transition oxide films were analyzed. They were a few microns thick.

3. Experimental results

The precipitates present in the metallic matrix of Zircaloy-4 and alloy 4 are mainly $Zr(Fe, Cr)_2$ and $Zr(Fe, V)_2$ Laves phases with hcp crystallographic structure and with Fe/Cr and Fe/V ratio respectively close to 1.7 and 1.9. These characteristics are in good agreement with those described in [10] for the same alloys. It is worth noting that, in both Zircaloy-4 and alloy 4, $Zr(Fe, Cr)_2$ and $Zr(Fe, V)_2$ amorphous precipitates were also observed in the α-Zr grains. They are characterized by a nearest neighbour spacing close to 2.2 Å (determined by electron diffraction). As reported previously [11], they are the consequence of a well-known artefact due to the ion milling.

The precipitates present in the metallic matrix of alloy 5 are mainly fine β-Nb, as mentioned in [10] for the same alloy. Interestingly, no amorphous precipitates were observed in the metallic matrix of the alloy 5, in contrast with the two above alloys (Zircaloy-4 and alloy 4).

3.1. Oxidation of $Zr(Fe, Cr)_2$ precipitates in Zircaloy-4

In the oxide film, three types of precipitates were observed:

- Three unoxidized precipitates (Fig. 1): they have the same crystalline structure (hcp) and Fe/Cr ratio (1.7) as in the precipitates present in the metallic matrix. These precipitates are located in the inner part of the oxide film, up to about 300 nm from the metal–oxide interface.
- Two amorphous precipitates (Fig. 2): their Fe/Cr ratio are close to 1.7 and their nearest neighbour spacing is equal to 2.2 Å. These characteristics are similar to the characteristics of ion milling amorphous precipitates. This suggests that their amorphization could have occurred during the thin foil preparation. These precipitates, which are then suspected to be non-amorphous and unoxidized before the ion milling, are located at 200 nm from the metal–oxide interface.
- One precipitate composed of equiaxed nanocristallites (<5 nm) (Fig. 3). This precipitate is located at 350 nm from the metal–oxide interface. The Fe/Cr

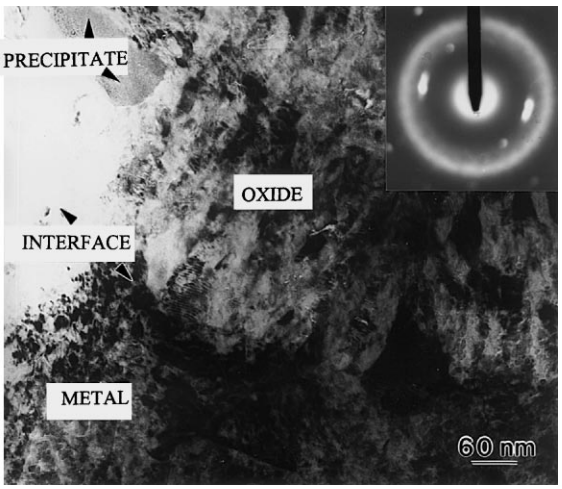

Fig. 2. Amorphous precipitate observed in the Zircaloy-4 oxide film, at about 200 nm from the metal–oxide interface.

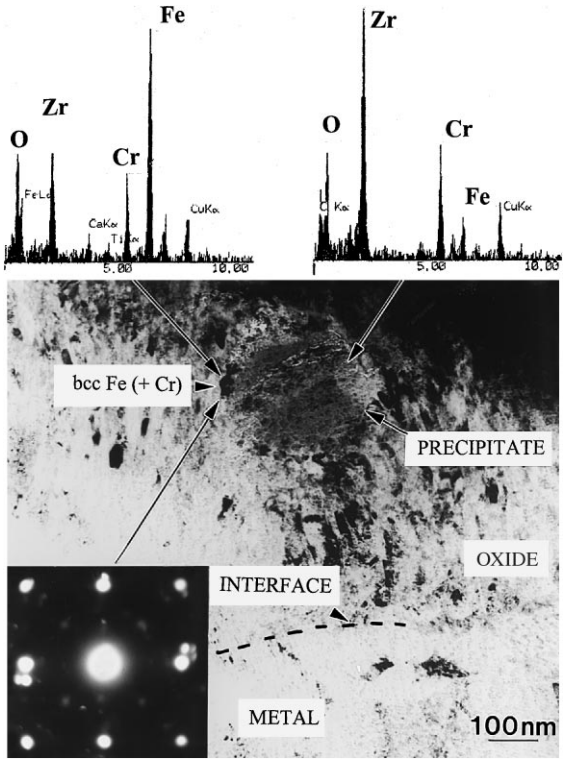

Fig. 3. Oxidized precipitate observed in the Zircaloy-4 oxide film, at about 350 nm from the metal–oxide interface. Local iron depletion and iron enrichment areas are observed in the precipitates. The latter area is identified by electron diffraction as a bcc iron–chromium phase.

ratio is ranging between 0.4 and 3.5, indicating a high evolution of the iron concentration inside the precipitate. The segregation of iron was identified by nano electron diffraction as metallic bcc iron–chromium phase.

3.2. Oxidation of $Zr(Fe, V)_2$ precipitates in alloy 4

Six precipitates were observed in the oxide film:

- Three of them are unoxidized precipitates (Fig. 4). They have the same crystalline structure (hcp) and Fe/V ratio (1.9) as in the precipitates present in the metallic matrix. These unoxidized precipitates are located at about 300 nm from the metal–oxide interface.
- The three other precipitates are amorphous (Fig. 5). They are located at more than 1 μm from the metal–oxide interface. Their Fe/V is ranging between 0.1 to 0.4 with a very low iron content (≈5%). The nearest neighbour spacing determined by electron diffraction is close to 2.8 Å. Since the characteristics of these amorphous precipitates (both Fe/V ratio and nearest neighbour spacing) are different from the characteristics of the ion milling induced amorphous precipitates [11], we can consider that the former are not the consequence of the ion milling. Moreover, since oxygen is detected inside the precipitates, we can assume that the amorphous precipitates located in the oxide film are oxidized, certainly as an amorphous zirconia.

3.3. Oxidation of β-Nb precipitates in alloy 5

Height precipitates were observed in the zirconia:

- Four of them are unoxidized (Fig. 6). Their aspect is similar to the aspect of precipitates present in the metal. Their niobium contents are close to 60%. The theoretic level (80% for β-Nb phase) is not obtained, maybe, because of the contribution of the matrix due to the small size of the precipitates (≈50 nm) compared to the size of the electron beam (≈70 nm) and to the thickness of the thin foil (⩽150 nm). The unoxidized precipitates are located up to about 400 nm from the metal–oxide interface.
- The four other precipitates are amorphous (Fig. 7). Their niobium contents are between 10% and 50%. Due to the small size of the precipitates, no measurement of the nearest neighbour spacing was possible. However, as no amorphous precipitates were observed in the metallic matrix, we can assume that they are not the consequence of an ion milling artefact. The amorphous precipitates are located between 0.35 and 2 μm from the metal–oxide interface.

Remark. The results described above were obtained on one thin foil made from each material. Note that, for Zircaloy-4 and alloy 5, they were reproduced on 3 other thin foils (made from each material).

4. Discussion

4.1. Alloying elements in the inner oxide layer

Previous TEM studies have shown that the oxidation of $Zr(Fe, Cr)_2$ precipitates was delayed compared to the zirconium matrix [1,2,4,5]. However since the examinations were conducted on frontal thin foils (metal–oxide interface parallel to the observation plane), it was not possible to locate precisely the precipitates in the oxide layer and, in particular, to quantify the distance between unoxidized precipitates and the metal–oxide interface. The present work performed on cross-sectional thin foils confirmed the previous results, unoxidized precipitates being found in the oxide film. In addition, it shows that unoxidized $Zr(Fe, Cr)_2$ precipitates are present up to about 300 nm from the metal–oxide interface (for such thin foils, the observation plane being perpendicular to the metal–oxide interface).

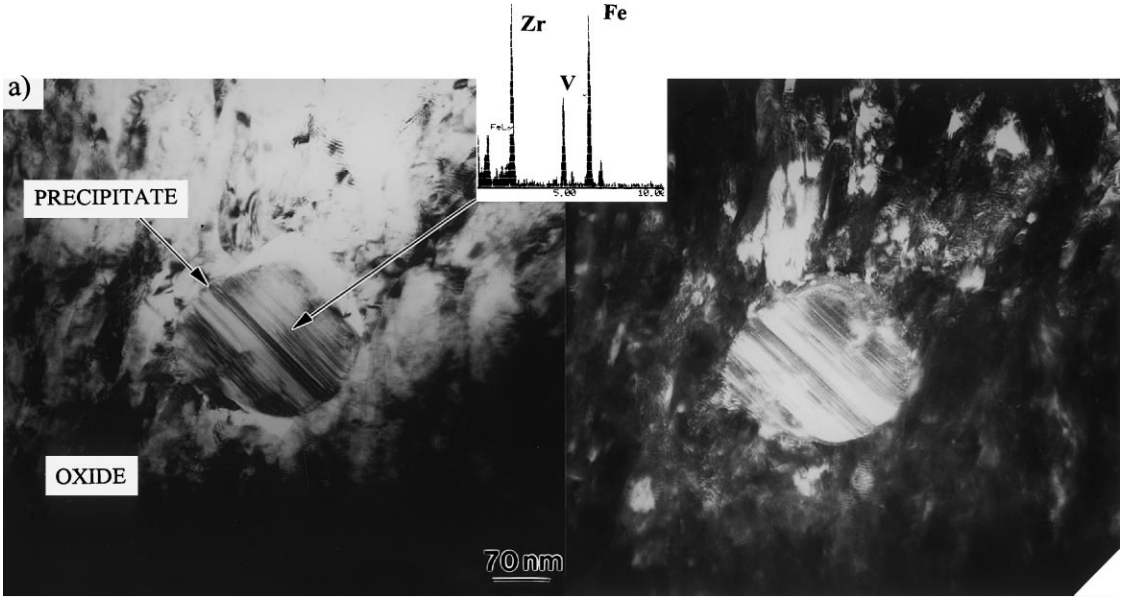

Fig. 4. Unoxidized $Zr(Fe, V)_2$ precipitate observed in the alloy 4 oxide film, at about 300 nm from the metal–oxide interface: (a) bright field and (b) dark field of the precipitate.

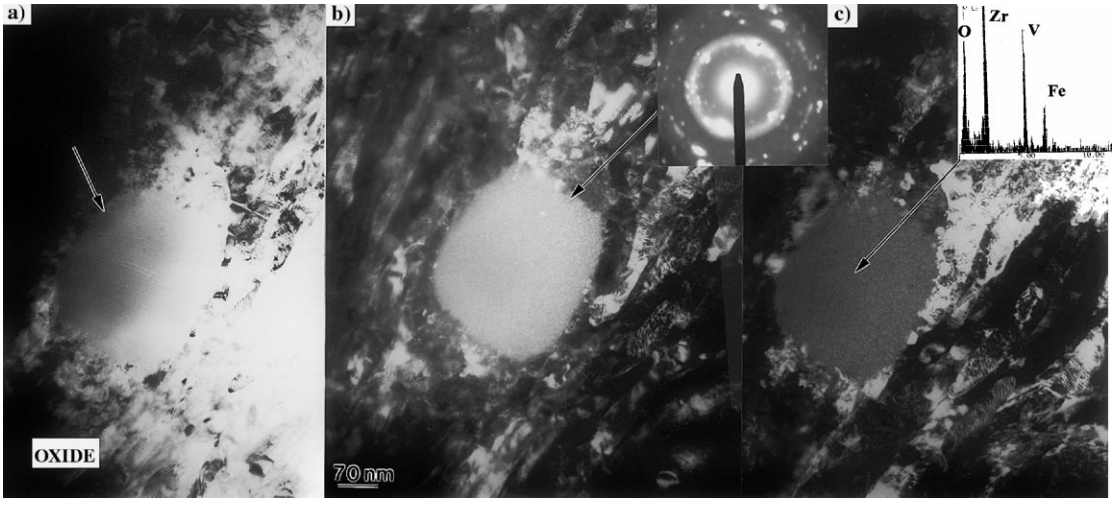

Fig. 5. Amorphous precipitate observed in the alloy 4 oxide film, at more than 1 μm from the metal–oxide interface: (a) bright field and (b) dark field of the precipitate, (c) dark field of the oxide grains.

Concerning the other types of precipitates present in advanced Zr-based alloys: β-Nb and $Zr(Fe, V)_2$ precipitates, it clearly appears that their oxidation is delayed compared to the zirconium matrix, up to at least 300 nm from the metal–oxide interface. It is similar to that observed for $Zr(Fe, Cr)_2$ precipitates.

The presence of unoxidized precipitates ($Zr(Fe, Cr)_2$, β-Nb and $Zr(Fe, V)_2$) in the inner oxide layer leads to the two following remarks:

- The existence of unoxidized precipitates in the oxide means that, not only their crystalline structure but, also their chemical composition, are similar to those determined in precipitates located in the metallic matrix. In another terms, neither iron, chromium, vanadium nor niobium dissolution (from the precipitates) into the zirconia occurs in the inner part of the oxide film. Therefore, in the inner oxide layer located from 0 to about 300 nm from the metal–oxide interface, no

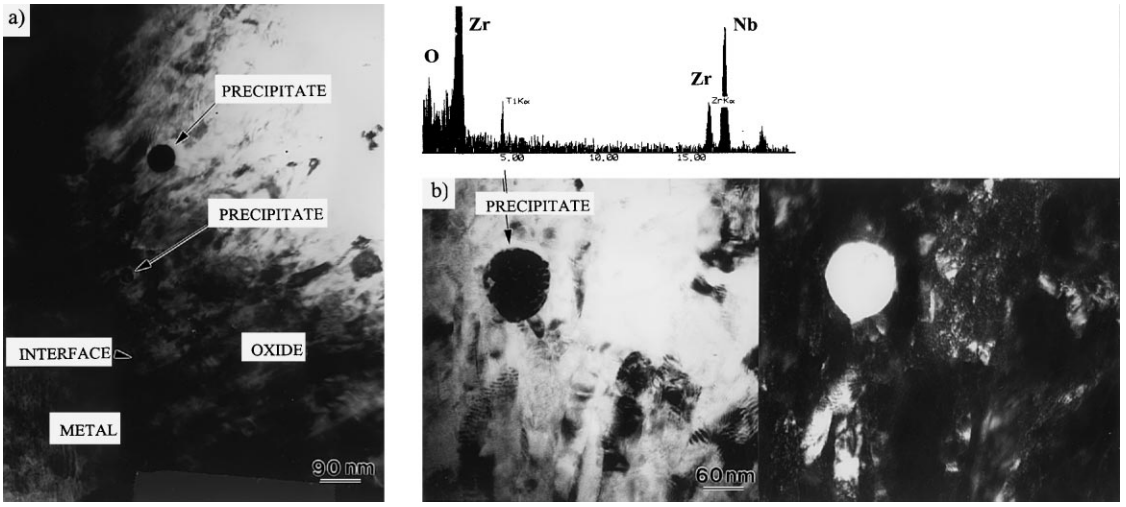

Fig. 6. Unoxidized β-Nb precipitates observed in the alloy 5 oxide film, at about 400 nm from the metal–oxide interface: (a) low magnification of the metal–oxide interface, (b) bright and dark fields focused on a β-Nb precipitate.

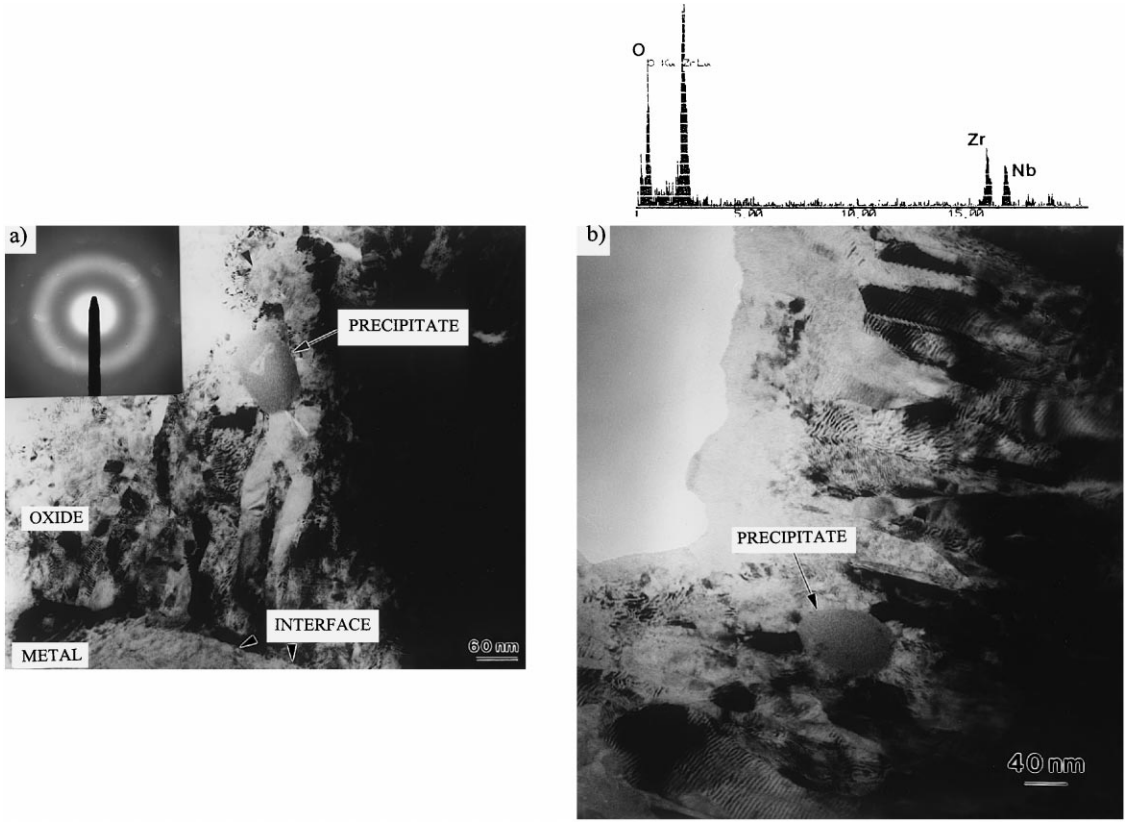

Fig. 7. Amorphous precipitates observed in the alloy 5 oxide film at about 350 nm (a) and 1 μm (b) from the metal–oxide interface.

chemical effect of the alloying elements present in the precipitates (Fe, Cr, V and Nb) is expected on the properties of the oxide, such as stabilizing the tetragonal zirconia phase or changing the conduction properties of the oxide. For instance, we can assume that the high tetragonal zirconia fraction detected close to

the metal–oxide interface [12] is not due to the iron alloying element but to the high compressive stresses induced by the oxidation of zirconium.
- The presence of metallic particles in the oxide film can modify the hydrogen transport in the oxide film. In particular, the assumption that Zr(Fe, $Cr)_2$ intermetallic precipitates could act as a fast transport route of hydrogen as a consequence of its metallic state in oxide film [13] can be extended to the other types of precipitates β-Nb and Zr(Fe, $V)_2$ present in advanced Zr-based alloys, the two latter remaining also unoxidized in the inner oxide layer.

4.2. Alloying elements in the bulk and outer oxide layer

In the bulk of the oxide layer, at a few hundred nanometers away from the metal–oxide interface, when the precipitates oxidize, their chemical composition evolves. In particular, the iron content in both Zr(Fe, $Cr)_2$ and Zr(Fe, $V)_2$ precipitates decreases. This observation indicates that some iron dissolves from the precipitates into the surrounding zirconia. In contrast, no significant evolution of the chromium and vanadium contents is observed inside the precipitates.

Therefore, if we can assume that the alloying elements Fe, Nb, V and Cr (contained in the precipitates) have not effect on the properties of the inner oxide layer, we can expect that iron can modify the bulk and the outer part of the oxide film (at more than 300 nm from the metal–oxide interface), as a consequence of its dissolution in the zirconia during the oxidation. For instance, iron which is known to stabilize the T–ZrO_2 [14], can delay the tetragonal to monoclinic transformation or change the conduction properties.

5. Conclusion

The main results dealing with the incorporation of Zr(Fe, $Cr)_2$, Zr(Fe, $V)_2$ and β-Nb precipitates into the oxide films formed on advanced Zr-based alloys in primary water at 633 K are the following:
- The oxidation of the three precipitates is delayed compared to the zirconium matrix.
- In the inner part of the oxide layer, up to about 300 nm from the metal–oxide interface, the precipitates remain unoxidized and no alloying element dissolution (Fe, Cr, V and Nb) occurs from the precipitates into the surrounding zirconia matrix.
- In the bulk of the oxide layer, at more than about 300 nm away from the metal–oxide interface, the precipitates oxidize and an iron depletion is observed in both Zr(Fe, $Cr)_2$ and Zr(Fe, $V)_2$ precipitates.

These results suggest that:
- the alloying elements present in the precipitates can not modify the inner oxide grain properties (such as stabilising the T–ZrO_2 phase or changing the conduction properties) because they remain entirely in the precipitates. In contrast, at a few hundred nanometers from the metal–oxide interface, iron can modify the above oxide properties, as a consequence of its partial dissolution from the precipitates into the surrounding zirconia matrix.
- The three types of precipitates can all modify the hydrogen transport through the oxide film because of their metallic state in the inner oxide film.

Acknowledgements

The authors would like to thank Science et Surface Society (Lyon, France) for TEM analyses and, especially, François Bossut for his expert cross-sectional thin foil preparation. They would like also to thank Framatome and EDF for financial support.

References

[1] E.R. Bradley, R.A. Perkins, in: Proceedings of IAEA Technical Committee Meeting on Fundamental Aspects of Corrosion of Zirconium Base Alloys in Water Reactor Environments, Portland, September 11–15, 1989, IWGFPT/34 International Atomic Energy Agency, Vienna, 1990, p. 101.
[2] T. Kubo, M. Uno, in: C. Eucken, A.M. Garde (Eds.), Zirconium in the Nuclear Industry, Ninth International Symposium, ASTM STP 1132, American Society for Testing and Materials, Philadelphia, 1990, p. 476.
[3] F. Garzarolli, M. Seidel, R. Tricot, J.P. Gros, in: C. Eucken, A.M. Garde (Eds.), Zirconium in the Nuclear Industry, Ninth International Symposium, ASTM STP 1132, American Society for Testing and Materials, Philadelphia, 1990, p. 395.
[4] D. Pêcheur, F. Lefebvre, A.T. Motta, C. Lemaignan, D. Charquet, in: A.M. Garde, E.R Bradley (Eds.), Zirconium in the Nuclear Industry, Tenth International Symposium, ASTM STP 1245, American Society for Testing and Materials, Philadelphia, 1994, p. 687.
[5] D. Pêcheur, F. Lefebvre, A.T. Motta, C. Lemaignan, J.F. Wadier, J. Nucl. Mater. 189 (1992) 318.
[6] Y. Hatano, M. Sugisaki, J. Nucl. Sci. Technol. 33 (11) (1996) 829.
[7] Y. Hatano, M. Sugisaki, J. Nucl. Sci. Technol. 34 (3) (1997) 264.
[8] J. P. Mardon, D. Charquet, J. Senevat, in: A.M. Garde, E.R Bradley (Eds.), Zirconium in the Nuclear Industry, Tenth International Symposium, ASTM STP 1245, American Society for Testing and Materials, Philadelphia, 1994, p. 615.
[9] J.P. Mardon, D. Charquet, J. Senevat, in: G.D. Moan (Ed.), Zirconium in the Nuclear Industry, Twelveth Inter-

national Symposium, ASTM STP 1354, American Society for Testing and Materials (to be edited).
[10] D. Gilbon, A. Soniak, in: Zirconium in the Nuclear Industry, Twelth International Symposium, ASTM STP 1354, American Society for Testing and Materials (to be edited).
[11] D. Pêcheur, A.T. Motta, C. Lemaignan, J. Nucl. Mater. 195 (1992) 221.
[12] J. Godlewski, L. Fayette, P. Bouvier, G. Lucazeau, in: G.D. Moan (Eds.), Zirconium in the Nuclear Industry, Twelth International Symposium, ASTM STP 1354, American Society for Testing and Materials (to be edited).
[13] Y. Hatano, K. Isobe, R. Hitaka, M. Sugisaki, J. Nucl. Sci. Technol. 33 (12) (1996) 994.
[14] S. Davidson, R. Kershaw, K. Dwight, A. Wold, J. Solid State Chem. 73 (1988) 47.